

NINETEENTH EUROPEAN ROTORCRAFT FORUM

Paper n° C7

PREDICTION OF YAW CONTROL EFFECTIVENESS  
AND TAIL ROTOR LOADS

by

Venkataraman Srinivas

Inderjit Chopra

Center for Rotorcraft Education and Research  
Department of Aerospace Engineering  
University of Maryland, College Park, MD 20742, USA

David Haas

Kelly McCool

Sea Based Aviation Office  
David Taylor Model Basin, Carderock Division, NSWC  
Bethesda, MD 20084, USA

September 14-16, 1993  
CERNOBBIO (Como)  
ITALY

ASSOCIAZIONE INDUSTRIE AEROSPAZIALI  
ASSOCIAZIONE ITALIANA DI AERONAUTICA ED ASTRONAUTICA



# Prediction of Yaw Control Effectiveness and Tail Rotor Loads

Venkataraman Srinivas\*                      Inderjit Chopra\*\*  
Center for Rotorcraft Education and Research  
Department of Aerospace Engineering  
University of Maryland, College Park, MD 20742, USA

David Haas†                                      Kelly McCool†  
Sea Based Aviation Office  
David Taylor Model Basin, Carderock Division, NSWC  
Bethesda, MD 20084, USA

## Abstract

The yaw control effectiveness of a helicopter in low speed flight at different headings is investigated. The SH-2 servo-flap controlled helicopter is modeled with the University of Maryland Advanced Rotor Code (UMARC) and the predicted trim results are correlated with flight test data. The velocities induced by the isolated main rotor wake below and behind the main rotor are correlated with experimental data. A comprehensive tail rotor model capable of predicting the tail rotor thrust under any combination of axial and edgewise flow is developed. The predicted tail rotor thrust is correlated in hover and in low speed flight at different heading angles. An empirical tail rotor/vertical fin interaction model is developed from available wind tunnel data. Predictions of the SH-2 trim pedal position with the isolated tail rotor alone as well as including the main rotor wake and tail rotor/fin interactions are obtained and correlated with flight test data. The isolated main rotor wake induces considerable velocities at the tail rotor location and, when included in the analysis, has a significant effect on the predictions of pedal position. The tail rotor/fin interactions affect the predictions of pedal position considerably in right sideward flight, particularly at speeds above 25 knots.

## NOTATION

$\mu$	advance ratio	$V$	wind velocity
$R$	main rotor radius	$V_x$	longitudinal velocity in body axes, positive rearward
$\Omega$	main rotor rotational speed, rad/sec	$V_y$	lateral velocity in body axes, positive to advancing side (right, as seen from top)
$v_i$	induced velocity at the rotor disk	$V_z$	vertical velocity in body axes, positive up
$v_h$	induced velocity at the rotor disk in hover	$\delta(\psi)$	servo-flap control input, fn. of azimuth
$V_v$	effective climb velocity (normal to tail rotor disk)	$T$	rotor thrust
$V_t$	forward flight velocity (edgewise, tangential to tail rotor disk)	$\rho$	density of air
$C_T$	thrust coefficient	$A$	rotor disk area
$\sigma$	rotor solidity	$K_p$	empirical factor to account for non- uniform inflow, rotational losses
$\psi$	azimuth angle of the rotor blade	$C_{sf}$	empennage side force coefficient

---

Presented at the Nineteenth European Rotorcraft Forum, Cernobbio (Como), Italy, Sept. 14-16 1993.

\* Graduate Research Assistant

\*\* Professor

† Aerospace Engineer

## INTRODUCTION

Low speed directional control characteristics for single main rotor helicopters are determined primarily by the capability of the tail rotor. The principle role of the tail rotor is to balance main rotor torque and provide adequate directional control. The tail rotor is expected to perform this function under a broad range of flight conditions. This can become a particularly challenging task at low airspeeds with side winds.

The tail rotor operates in a very complex aerodynamic environment as a result of a combination of factors including the forward flight of the helicopter, sidewind velocity and interaction with the main rotor wake and vertical fin [1] - [4]. Inflow angles at the tail rotor encompass a wide variation due to operation in the vortex ring state, the wind mill brake state, as well as the normal working state. On the other hand, the main rotor operates largely as an isolated rotor in the normal working state.

Interactional effects occur because the tail rotor must operate directly in the wake of the main rotor and in close proximity to the vertical fin. The severity of the aerodynamic interactions from the main rotor wake depends on the location of the tail rotor with respect to the main rotor, characteristics of the main rotor and flight condition. In hover, the tail rotor operates in an axial flight condition (when no wind is present). The main rotor wake normally does not interact significantly with the tail rotor in this condition. In forward flight, the edgewise flow on the tail rotor decreases the velocity induced by the tail rotor in generating the same amount of thrust. Also, the main rotor wake causes a downwash velocity and a considerable increase in the edgewise flow on the tail rotor disk. The wake also induces a considerable out-of-plane inflow on the tail rotor.

Figure 1 shows the top view of a helicopter in yawed flight. The heading angle is defined such that right sideward flight (RSF) corresponds to 90° and left sideward flight (LSF) corresponds to 270°. When the helicopter is in sideward flight or in a sideslip, there is a considerable component of velocity in the inflow direction of the tail rotor. For a sidewind from the right (U.S. rotors), the tail rotor operates in a state equivalent to a main rotor in "climb". As the sidewind velocity increases, the velocity induced by the tail rotor for generating the same

amount of thrust decreases. For a sidewind from the left, the rotor operates in the "descent" condition. For a low sidewind speed, a definite slipstream exists at the tail rotor disk, i.e., normal working state of the rotor. For increasing sidewinds from the left, a definite slipstream ceases to exist at the tail rotor disk. This state where the rotor tip vortices stay very close to the rotor blades is characterized by high vibration and stall phenomena and is called the vortex ring state. This state is characterized by a large increase in the induced velocity which results in a large reduction in the tail rotor thrust at a given collective pitch setting. A small change in the inflow velocity could plunge the tail rotor into the vortex ring state; consequently a sudden loss of yaw control would be experienced by the pilot. For higher sidewinds from the left, the slipstream forms again since the descent velocity is far greater than the velocity induced at the tail rotor disk. This is referred to as the windmill brake state. All the above effects have to be taken into consideration in predicting the tail rotor thrust and consequently the yaw control characteristics of the helicopter.

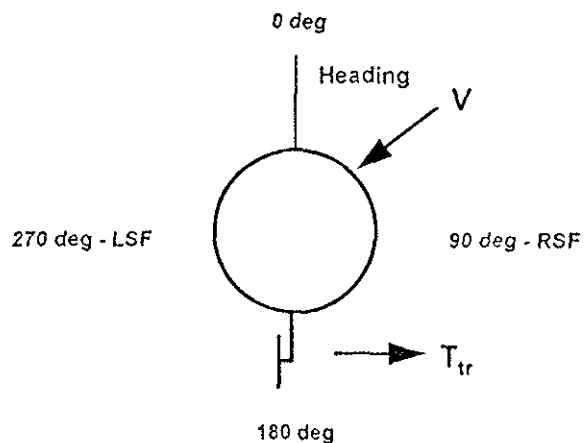


Fig. 1 Top view of single main rotor helicopter in yawed flight

The highest demands are placed on the tail rotor during low speed flight where main rotor torque is high and can change rapidly with small changes in airspeed. Because of side winds, relative winds can approach from any direction and can change rapidly as in the case of a helicopter maneuvering. This can result in large tail rotor thrust variations which increase pilot work load and reduce control effectiveness. Low speed flight is also demanding because it is difficult to ascertain ambient wind conditions which determine

aircraft heading and true airspeed without an accurate omnidirectional airspeed system. Thus, pilots often resort to flying in a ground reference system. A further complication of the low speed flight environment is that it typically involves a demanding mission that requires the pilot's attention outside the cockpit such as locating an object on the ground or in the water. These conditions, either alone or in combination, can create a situation conducive to a loss of aircraft directional control.

Several single main rotor helicopters have experienced directional control limitations in low speed flight [5]. The U.S. Army has experienced a series of incidents on a light scout helicopter involving an uncommanded right yaw and loss of aircraft yaw control during low speed flight. These incidents led to an investigation of loss of tail rotor effectiveness (LTE) on the OH-58 helicopter [6]. The investigation found that LTE can occur to a varying degree on any single rotor helicopter. Both wind tunnel and flight test were conducted and the results are summarized in Ref. [6]. Three critical factors that can contribute to loss of aircraft directional control were identified; the tail rotor operating in the vortex ring state, the influence of main rotor tip vortices on the inflow at the tail rotor, and fuselage weathercock instability in rearward flight.

Wind tunnel test of the OH-58 [7] showed that for wind speeds of approximately 35 to 45 knots at certain wind azimuth directions, a sufficient yaw moment could not be achieved at maximum tail rotor collective to maintain aircraft trim. The cause was attributed to reduced tail rotor thrust due to wind azimuth direction in combination with an adverse pressure suction force on the vertical fin of the aircraft.

As part of the investigation reported in Ref. [6], an evaluation for a modified tail rotor of the OH-58 to provide additional directional control authority was conducted and pilot corrective actions were recommended to overcome an uncommanded right yaw situation. The corrective action consists of adding left pedal and forward cyclic until control is regained. Training to increase pilot situational awareness was also encouraged.

Directional control difficulties encountered during low speed flight near the ground (i.e., in ground effect) have also been investigated.

Wind tunnel studies on tail rotor loads showed that with a rearward wind, a sudden loss in tail rotor thrust can occur [5]. This is caused by the interaction of the tail rotor with a ground vortex generated by the main rotor wake impinging on the ground. It was found that changing the tail rotor direction of rotation significantly improved tail rotor performance in this condition.

Several flight incidents involving loss of aircraft directional control have also been experienced by U.S. Navy pilots [8, 9, 10]. In Ref. [9], one such incident was described in which the aircraft encountered an unanticipated right yaw (URY) resulting in the aircraft rapidly spinning several revolutions. A discussion of some of these incidents is provided in Ref. [10] along with a review of the conditions in which loss of directional control can occur. Typically, they involve low speed flight with changing wind direction. Low speed critical azimuth flight test results were analyzed in Ref. [10] in terms of minimum, maximum, and average values of control position for varying heading and airspeed. For some combinations of heading and airspeed, large variations in pilot control positions can occur due to the unsteady flow environment at the tail rotor.

Flight test investigation into tail rotor aerodynamics have also been conducted by the Defense Research Agency at Bedford England using an instrumented Lynx AH Mk5 helicopter in an effort to improve yaw control characteristics of that aircraft in the low speed flight environment [11].

Various approaches have been investigated to improve direction control of single main rotor helicopters in low speed flight. One example is the use of a strake attached to the tail boom. Both wind tunnel [12] and flight tests [13] have been conducted to evaluate the effectiveness of using a strake to change air loads on the tail boom for improving low speed directional control characteristics. Currently, several European helicopters are now flying with tail boom strakes. Other approaches include modifications to the tail rotor to increase thrust, alteration of the vertical fin location and size, change in the direction of tail rotor rotation, as well as increased pilot training for improved situational awareness. In addition, alternative designs such as fenestrans and NOTAR tail booms are being utilized in order to eliminate

some of the inherent difficulties encountered with conventional tail rotors.

The purpose of the present study is to develop an analytical model from which to better understand some of the phenomena that can lead to low speed directional control difficulties. Specifically, the effect of the main rotor tip vortices on tail rotor thrust for various airspeed and azimuth combinations is examined. A servo flap controlled main rotor model with a complex free wake is developed using the University of Maryland Advanced Rotorcraft Code (UMARC) [14]. Main rotor wake velocities at the tail rotor plane are calculated and a blade element tail rotor representation is used to calculate trim control positions. Tail rotor inflow is based on momentum theory with an empirical correction for the vortex ring state. An empirically-based vertical fin correction factor is also developed based on wind tunnel data. Analysis of an isolated tail rotor is compared with wind tunnel test data for an OH-58 tail rotor and results for complete aircraft trim are compared with full scale critical azimuth flight test data for a Navy/Kaman SH-2F helicopter.

## TECHNICAL APPROACH

The analysis consists of four phases that involve calculation of: the vehicle coupled trim, the effect of the main rotor wake at the tail rotor disk, the induced inflow and thrust of the tail rotor, and the interaction between the tail rotor and vertical fin. For results, the SH-2 helicopter is selected. It is a 4-bladed rotor with servo flaps for primary controls.

### Vehicle Trim Solution

The trim analysis involves the calculation of the control positions, vehicle orientation and the blade response. The blade is assumed as an elastic beam undergoing flap bending, lag bending, elastic twist and axial deformation. It is discretized into a number of finite elements, with each element consisting of 15 degrees of freedom. The blade nonlinear finite element equations are then transformed to the modal space using coupled natural modes. Steady periodic response of the blades is calculated using the finite element in time approach. The blade response equations and vehicle trim equations are solved iteratively as a coupled set

of equations. The vehicle trim equations are solved by calculating a Jacobian matrix at the initial guess of trim controls and the update of trim controls is done using a Newton-Raphson approach. The trim solution is obtained when the resultant steady forces and moments on the vehicle become zero.

To calculate the trim solution of the SH-2 helicopter in forward flight, UMARC is modified to better reflect the characteristics of the servo-flap controlled main rotor [15,16]. The trim variables for a conventional helicopter are two shaft orientation angles  $\alpha_s$  and  $\phi_s$ , the main rotor collective pitch  $\theta_0$ , cyclic pitch  $\theta_{1c}$  and  $\theta_{1s}$ , and the tail rotor collective pitch  $\theta_t$ . For the servo-flap main rotor, the primary rotor controls become the servo-flap collective  $\delta_0$  and the servo-flap cyclic inputs  $\delta_{1c}$  and  $\delta_{1s}$ . The control angle input to the blade is

$$\delta(\psi) = \delta_0 + \delta_{1c} \cos\psi + \delta_{1s} \sin\psi$$

The servo-flap on the SH-2 is an external airfoil flap placed at the trailing edge on each blade between 65.8% and 82% of the blade span. The SH-2 rotor blades are twisted with a nose-up preset angle of 27° at the root. This pretwist is much higher than is required to trim the helicopter in any flight condition. But as the rotor is accelerated to its rotational speed, the additional nose-down pitching moment generated by the servo-flap (at a zero deg. servo-flap angle), causes the elastic blade to twist nose-down thereby reducing the blade pitch angle by a considerable amount because of low torsional stiffness. Any application of servo-flap control input deflects the blade about this already elastically deformed position. The blade structural properties have been adequately modeled to reflect the large blade chordwise c.g. and a.c. offsets present in the servo-flap region. The blade aerodynamic sectional properties are modeled using a simple theory of flap sections [17] and utilize the SH-2 airfoil section data from Ref. [16]. The calculation of the rotor blade response and airloads are modified in UMARC to take into account these airfoil characteristics.

### Complete Aircraft Model

The collective servo flap angle of the SH-2 rotor ranges from 6.38 deg. (trailing edge down) at the zero control position to -9.37 deg. (trailing edge up) at the 100% position [15]. For the

longitudinal stick control, the range is -6.34 deg. (most aft) at the zero position to 17.66 deg. (most forward) at the 100% position. At the zero lateral stick position, the servo-flap deflects by -5.32 deg. and for the 100% position, it deflects by 5.32 deg. The total tail rotor collective range is 32 deg. The tail rotor pitch is at -6 deg. at the full right pedal position and at 26 deg. at the full left pedal position.

Main rotor and body characteristics for the SH-2 helicopter [16] are given in Table 1. In Figures 2 to 6, predicted trim results for the SH-2 helicopter are compared with flight test data [15].

Main rotor radius	22 ft.
Number of blades	4
Rotor disk area	1520.5 sq. ft.
Rotor blade mean chord	1.82 ft.
Rotor solidity	0.1052
Flap and lag hinge offsets	0.6875 ft.
Root cut-out	21.4 %
Servo flap total chord	0.7083 ft.
Distance from blade feathering axis to servo flap hinge axis	1.555 ft.
Blade mass (including servo flap)	8.90 slugs
Forward shaft tilt	6.0°
Lateral shaft tilt (left)	4.0°
Lock number, sea level	5.07
Gross Weight	12900 lb.

Table 1. Characteristics of the SH-2.

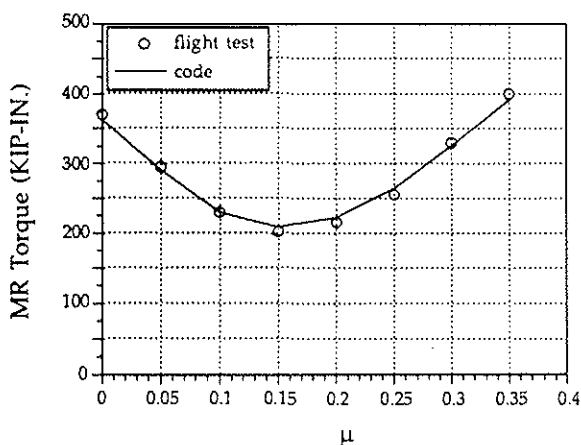


Fig. 2 SH-2 Main Rotor Torque ( $C_T/\sigma = 0.0725$ )

Good correlation of main rotor torque is essential for accurately predicting the tail rotor thrust required for vehicle trim and hence the pedal position. Figure 2 shows the comparison of main rotor torque predicted using UMARC with flight test data. The correlation is very good for all advance ratios. Figure 3 shows the comparison of the predicted main rotor collective servo-flap angle with flight data. Again, the correlation is quite satisfactory.

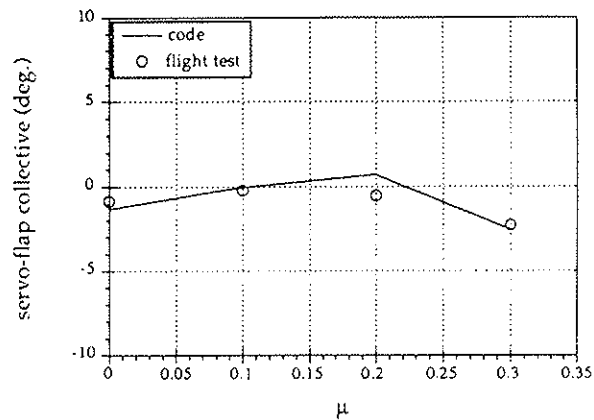


Fig. 3 SH-2 servo-flap collective angle (deg.)

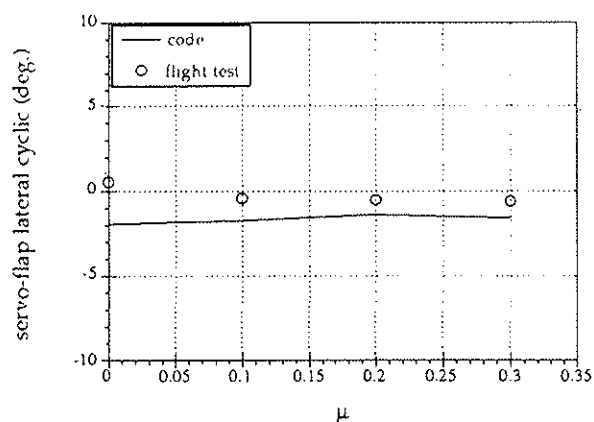


Fig. 4 SH-2 Lateral Cyclic Control (deg.)

The comparison of lateral and longitudinal cyclic controls with flight data is shown in Figures 4 and 5 respectively. Again, satisfactory correlation is obtained over all advance ratios. Figure 6 shows good correlation of the tail rotor collective over all advance ratios. This can be attributed to a satisfactory prediction of main rotor torque and an accurate tail rotor model in forward flight.

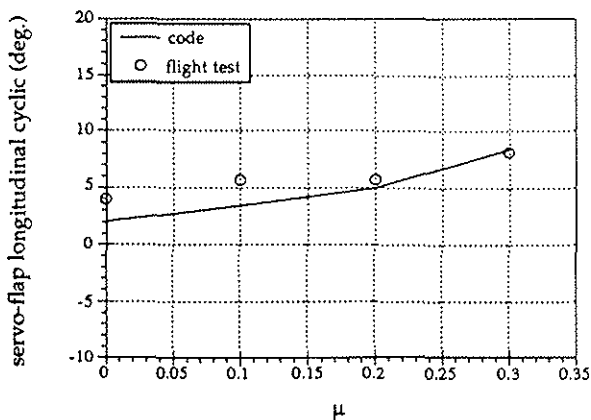


Fig. 5 SH-2 Longitudinal Cyclic Control (deg.)

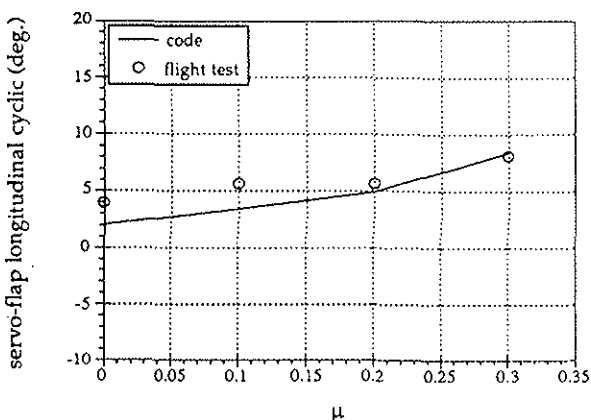


Fig. 6 SH-2 Tail Rotor Collective (deg.)

### Main Rotor Wake Model

The main rotor wake is an important and necessary ingredient for predicting loads on the main rotor as well as on the tail rotor [1] - [4], [18]. The main rotor wake may induce large velocities at the tail rotor disk, especially in low speed flight and plays a crucial role in determining the inflow at the tail rotor [5]. Prediction of correct trends and magnitudes of the induced flow-field of the main rotor is necessary to determine tail rotor loads accurately. As the helicopter transitions from hover to low speed forward flight, the main rotor tip vortices come in close proximity to one another. A considerable roll-up of the tip vortices from the rotor disk forms. The modeling of this phenomenon of the fixed-wing type roll-up of the rotor vortices is possible only by using the free-wake methodology. In UMARC, the wake roll-up is calculated using the Scully free-wake model [19] as implemented by Johnson [18]. In this model, the main rotor

blade tip vortices are broken up into elements and the location of these elements is determined by solving the coupled system, since the location of every vortex filament affects the location of every other vortex filament. This model prescribes the inboard wake with large core vortices and solves for the tip vortex geometry. The blade harmonic response and the time-dependent spanwise circulation distributions are given as inputs to the wake calculations. The resulting inflow distribution output from the wake model is used in calculating the blade response and trim controls [20]. The free-wake geometry calculated by this approach at the converged trim condition is then used for calculation of the induced flow field at the tail rotor location.

The free wake model has been validated extensively [21] in terms of the induced velocities at the rotor disk. However the interest in this analysis is to determine the induced velocity at the location of the tail rotor. Therefore, a comparison of the main rotor wake induced velocities below and behind the main rotor disk predicted using the free wake analysis in UMARC with experimental data is carried out. The data are from the University of Maryland's four-bladed rotor test [22] for an advance ratio of  $\mu=0.075$  and  $C_T/\sigma=0.075$ . Figure 7 shows the induced velocity in the lateral direction at a distance of  $0.29R$  directly below the main rotor hub. The analysis predicts the trends of the induced velocity variation very well but the oscillatory magnitudes are under-predicted.

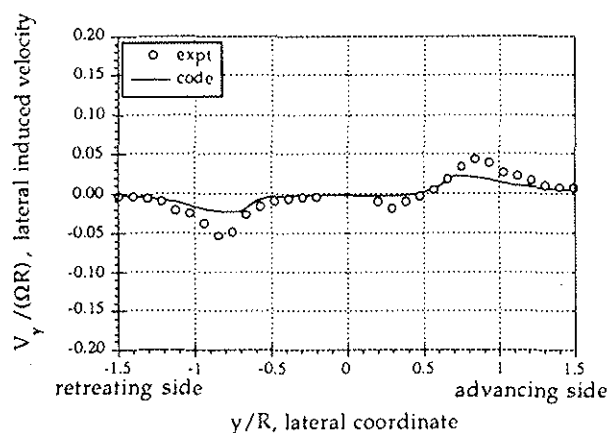


Fig. 7 Comparison of lateral velocities induced at  $0.29R$  below the main rotor hub

A comparison of the velocities behind the main rotor at a distance of  $1.05R$  from the main rotor hub and  $0.29R$  below the hub is shown in Figures 2.2 - 2.4.

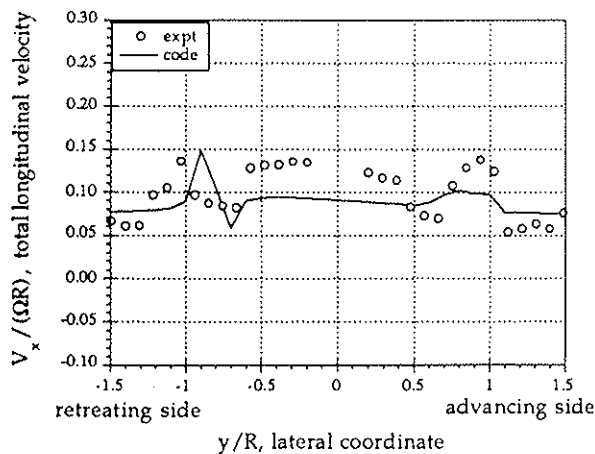


Fig. 8 Total longitudinal velocity 1.05R behind the main rotor (free stream plus induced velocity)

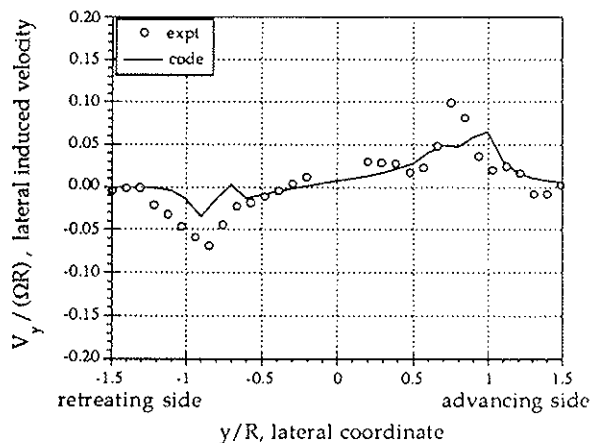


Fig. 9 Lateral induced velocity 1.05R behind the main rotor

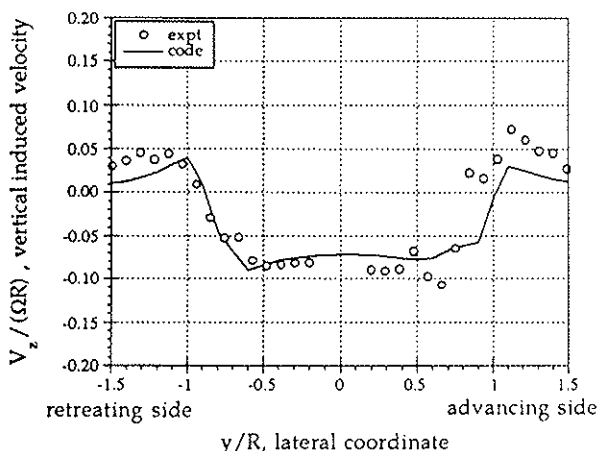


Fig. 10 Vertical induced velocity 1.05R behind the main rotor

Figure 8 shows the longitudinal induced velocity variation with the lateral coordinate. Here, too, the trends are predicted well, but the analysis does not predict the large deviation seen in the longitudinal velocity from the free stream velocity around the fuselage axis. Some of these deviations are probably due to the presence of the rotor hub and body which are not accounted for in the analysis. Figure 9 shows the variation of the lateral induced velocity at different lateral coordinates. The analysis predicts the trends and the magnitudes satisfactorily. The positive and negative peaks are due to the presence of the two rolled-up rotor tip vortices from the advancing and retreating sides respectively. The variation of the vertical induced velocity along the lateral coordinate is predicted very well in Figure 10. The lateral induced velocity acts as an additional inflow at the tail rotor and the longitudinal and vertical components act as edgewise flow components for the tail rotor disk.

#### Tail Rotor Inflow

When the helicopter is exposed to a sidewind, the tail rotor operates in an equivalent climb/descent condition in combination with the forward flight velocity. For moderate sidewinds from the left (for U.S. rotors), the tail rotor may experience a vortex ring state. Existing theoretical models cannot predict the inflow in this state of operation. Hence an empirical model is used [23]. The basis for this model is experimental data obtained from rotor tests in the vortex ring state. The model has also been extended to forward flight using a momentum theory approach [23]. For other sidewind conditions, the rotor is not operating in a vortex ring state, and the momentum theory is used to predict the induced inflow at the rotor disk.

Unlike the main rotor, the tail rotor experiences winds from all directions. Wind velocity and heading have a strong effect on the inflow at the tail rotor. In a pure axial flight condition, the rotor operates in one of three states, i.e., the normal working state ( $V_v/v_h > -0.5$ ), windmill brake state ( $V_v/v_h < -2.0$ ) or in the vortex ring state ( $-2.0 < V_v/v_h < -0.5$ ). The first two states are characterized by the presence of a slipstream at the rotor disk and the induced velocity is calculated using momentum theory:

$$v_i = v_h [-V_v / 2v_h \pm \sqrt{(V_v / 2v_h)^2 + 1}]$$

where  $v_h = K_p \sqrt{(T/2\rho A)}$  and  $K_p = 1.15$ .

The positive and negative signs respectively represent the normal working state and the windmill brake state. The windmill brake state is rarely encountered at the tail rotor due to the helicopter's sideward speed limitations.

The vortex ring state can be encountered at the tail rotor in low speed left sideward flight. This state is an unsteady flow condition where the freestream is of the same order of magnitude as the induced flow due the rotor but is in the opposite direction. This results in an unsteady condition where the flow recirculates around the rotor disk causing a very high induced velocity at the rotor which results in a sharp decrease in thrust for a given collective pitch. Momentum theory breaks down in this flow regime and an empirical model is used to predict the induced velocity in the vortex ring state [23].

$$v_i = v_h [ 1.419 (V_v/v_h)^3 + 3.672 (V_v/v_h)^2 + 1.798 (V_v/v_h) + 1.423 ]$$

In addition to the inflow variation in axial flight, the reduction of induced velocity as forward speed increases is modeled using a momentum theory based approach [23] as:

$$v_i = v_h / \sqrt{[(V_t/v_h)^2 + ((V_v+v_i)/v_h)^2]}$$

Figure 11 shows that increasing forward speed ( $V_t/v_h$ ) reduces the magnitude of the induced velocity and hence the severity of the vortex ring state.

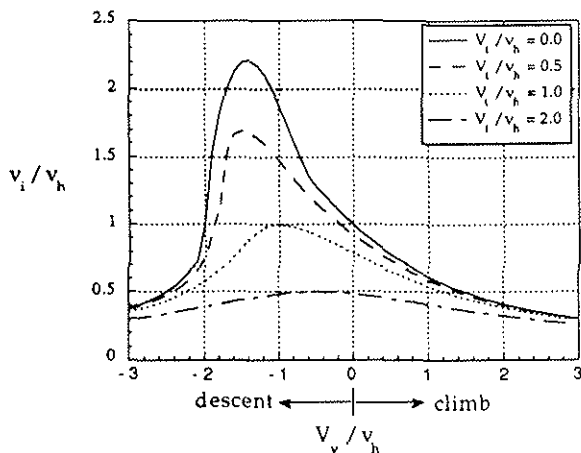


Fig. 11 Variation of induced velocity with climb and forward flight velocity

### Isolated Tail Rotor Model

An isolated tail rotor model has been developed using the inflow model described above to predict the variations in thrust under various wind conditions. The thrust is obtained by performing numerical integration over the blade elements along the blade radius and azimuth. The lift and drag components of each element are calculated to obtain the incremental normal force acting on the blade element. A blade root cut-out of 15% and a tip-loss correction factor of 94% have been used in the thrust calculations. Airfoil section lift and drag are calculated using NACA 0012 airfoil data with stall and compressibility effects.

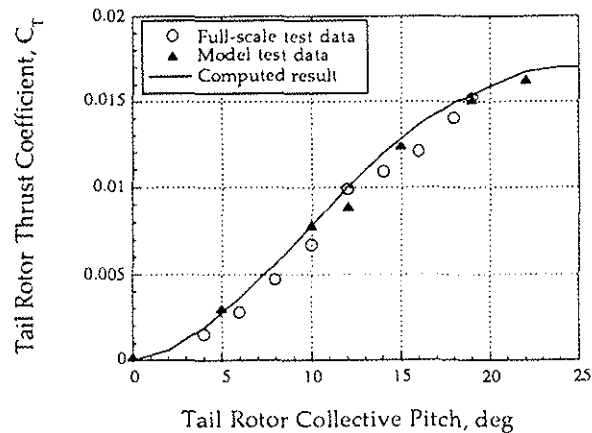


Fig. 12 Comparison of predicted OH-58 isolated tail rotor thrust coefficient in hover with test data

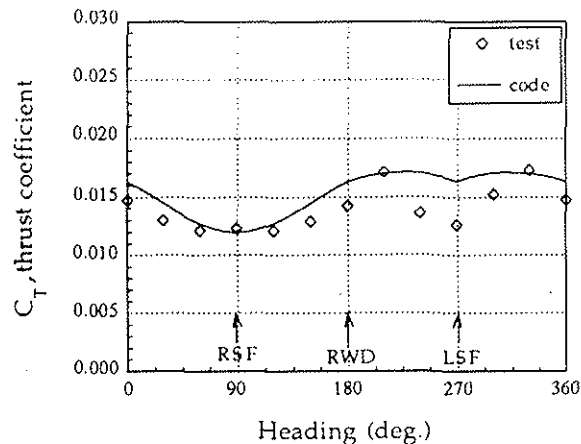


Fig. 13 OH-58 tail rotor thrust coefficient variation with heading (35 kts, collective = 19°)

An OH-58 tail rotor configuration is used in the isolated tail rotor analysis since wind tunnel data are available for correlation [7]. Figure 12 shows a good correlation of the predicted thrust

with wind tunnel and full scale test data in hover. Figures 13 and 14 show the variation in thrust coefficient of an OH-58 isolated tail rotor with heading at wind speeds of 35 and 45 knots respectively. The decrease in the thrust in left sideward flight (around 270°) is due to the operation of the rotor in the vortex ring state. The analysis predicts the vortex ring state effect quite well at 45 knots, whereas the correlation is not as good at 35 knots.

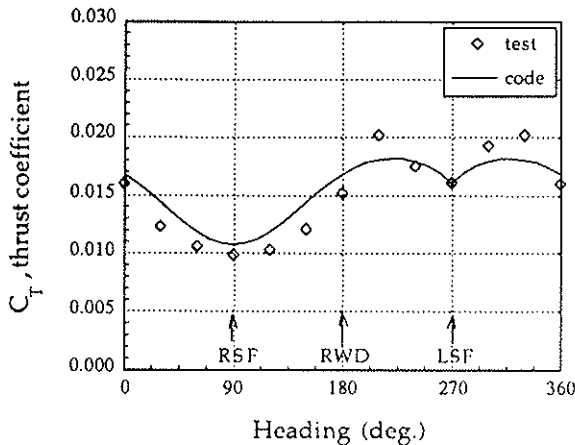


Fig. 14 OH-58 tail rotor thrust coefficient variation with heading (45 kts, collective = 19°)

An isolated SH-2 tail rotor has also been studied. Table 2 shows the comparison of the two rotor configurations.

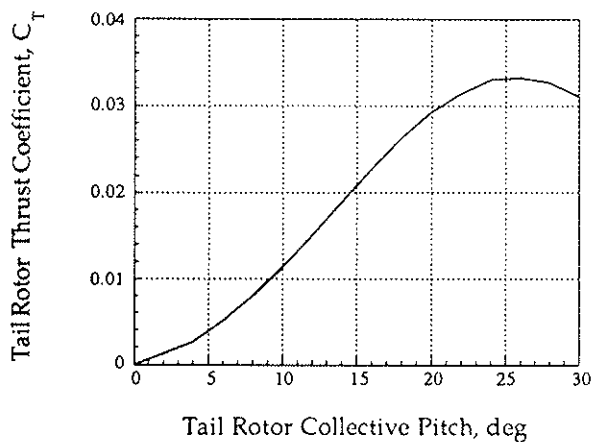


Fig. 15 Calculated isolated SH-2 tail rotor thrust coefficient in hover

Airfoil data for a NACA 0012 airfoil were used for both rotors. The predicted results for the SH-2 isolated tail rotor (Figures 15 and 16) are very similar in trend to the ones for the OH-58 and indicate the presence of the vortex ring

state at 35 and 45 knots for heading angles near 270°.

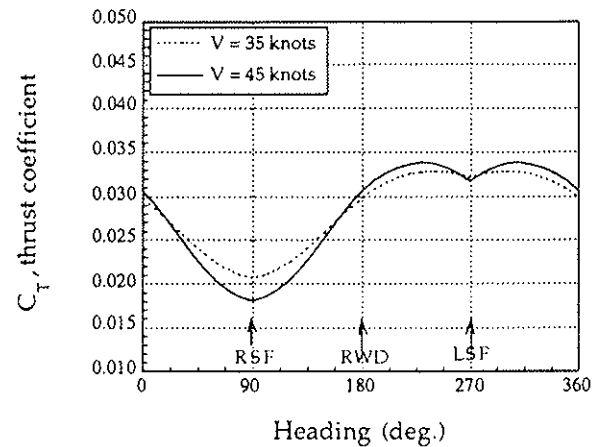


Fig. 16 SH-2 thrust coefficient variation with heading (collective = 19°)

OH-58	SH-2
R = 2.58 ft	R = 4.08 ft
$\sigma = 0.122$	$\sigma = 0.242$
No twist	-12° twist
2 blades	4 blades
63-015 airfoil section	63-012 airfoil section

Table 2. Comparison between the OH-58 and SH-2 tail rotor configurations

#### Tail Rotor / Vertical Fin Interference Effects

The tail rotor is usually mounted in close proximity to the vertical fin. The presence of the fin causes a blockage effect that decreases the induced inflow at the tail rotor thus increasing its thrust. Also, for pusher-type tail rotor configurations such as the OH-58 and the SH-2, the velocity induced at the tail rotor produces a suction effect on the side of the fin facing the tail rotor. This suction force causes an adverse yaw moment which the tail rotor thrust must counter in addition to the main rotor torque in order to maintain yaw equilibrium [5, 7, 24, 25, 26]. Since no theoretical models exist for prediction of this interaction, a tail rotor/fin correction methodology has been arrived at from the limited test data [7]. This correction accounts for both the increase in the tail rotor thrust due to the presence of the fin and the adverse fin force due to tail rotor operation for different flight velocities and heading angles.

## Vertical Fin Interaction Model

Modeling of the tail rotor/vertical fin interactions is quite challenging and this model is based solely on empirical methods. Two correction factors have been developed for the SH-2 by scaling the OH-58 fin effects obtained from wind tunnel tests. These correction factors account for: 1) an increase in tail rotor thrust due to vertical fin blockage and 2) an adverse fin force due to the tail rotor's proximity to the fin.

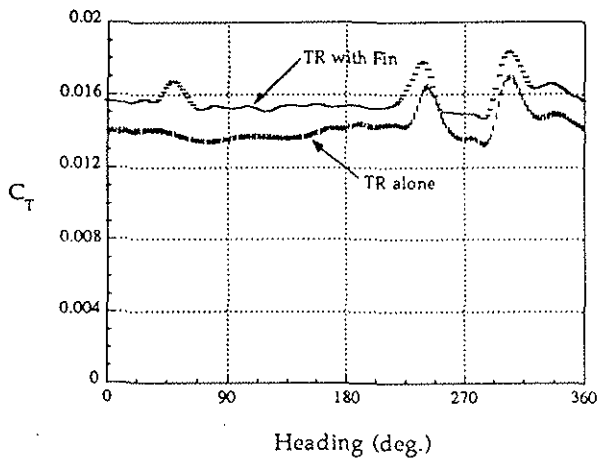


Fig. 17 Effect of Fin on OH-58 Tail Rotor Thrust Coefficient [7], collective = 19°, V = 20 knots

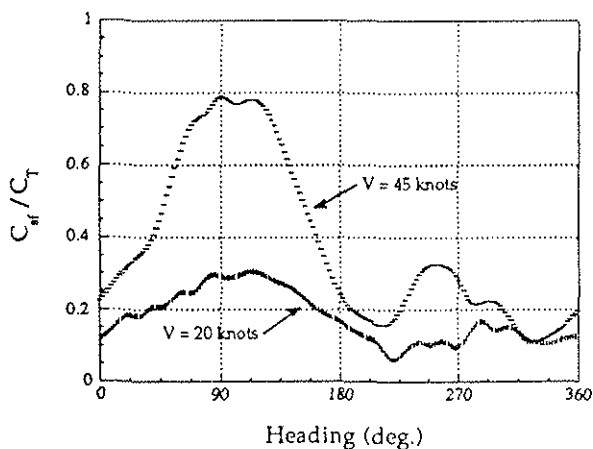


Fig. 18 Variation of OH-58 Empennage Side Force Coefficient as a ratio of tail rotor thrust coefficient, collective = 19°, blockage ratio = 0.44

The blockage effect of the fin on the tail rotor was determined for the OH-58 by measuring the tail rotor thrust at a particular wind speed and collective pitch and varying the heading in the wind tunnel [7]. Tail rotor thrust was measured under different conditions for tail rotor alone and tail rotor/fin combination. The

difference in measured thrust in Figure 17 corresponds to the increase in tail rotor thrust due to the presence of the OH-58 fin. At 20 knots and tail rotor collective of 19°, a change from a 10% blockage ratio (fin off for the OH-58) to a 44% blockage ratio (fin on for the OH-58) results in a 14% increase in thrust. Linear interpolation is applied to determine the change in thrust in going from zero blockage (fin off for the SH-2) to 21% blockage (fin on for the SH-2). Hence an increase in tail rotor thrust of 8.6% for the SH-2 has been arrived at, for all heading angles. This analysis assumes that the trend seen in Figure 17 is the same at other wind velocities and collective settings.

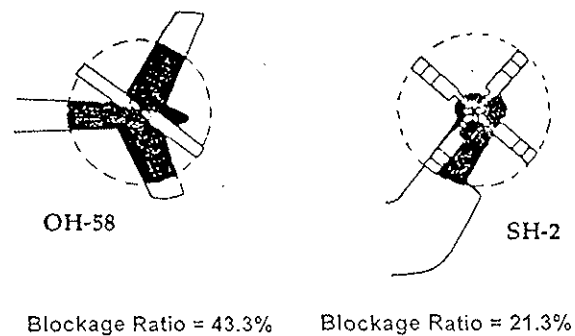


Fig. 19 Relative fin sizes of OH-58 and SH-2

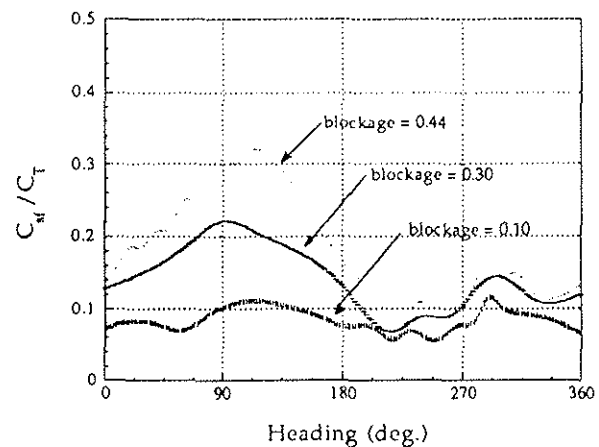


Fig. 20 Variation of OH-58 Empennage Side Force Coefficient as a ratio of tail rotor thrust coefficient with blockage ratio, collective = 19°, V = 20 knots

The adverse fin force, on the other hand, varies dramatically with heading. The variation with heading and windspeed of empennage side force as a percentage of thrust has been obtained from OH-58 wind tunnel data [7] (Figure 18). Linear interpolation is performed to obtain the correct OH-58  $C_{sf}/C_T$  at a

particular heading and wind speed. The sideforce is then linearly scaled for blockage ratio to obtain the  $C_{sf}/C_T$  value for the SH-2 (Figure 20). Thus, the adverse fin force obtained is a function of wind speed, heading, tail rotor thrust and blockage ratio.

### CRITICAL AZIMUTH RESULTS

Figures 21 to 25 show the variation in pedal position required with heading angle to maintain trim flight for relative winds from 20 to 45 knots. The first set of results (dotted line) are the pedal position predictions with no interaction effects. The second set of results (dash-dotted line) take into account the wind as well as the main rotor wake interaction at the tail rotor disk. The main rotor wake induced velocities have been averaged over five points on the tail rotor disk and contribute to the resultant velocity at the tail rotor. The third set of results (solid line) represent the pedal position predictions as a result of the wind velocity, main rotor wake effects at the tail rotor and the tail rotor/vertical fin interaction phenomena. Flight test data are also plotted on Figures 21 to 24. Unlike a wind tunnel test, an exact heading and airspeed cannot be maintained by the pilot during full scale critical azimuth flight testing. This is due to unsteady flow conditions present in low speed yawed flight. As a result, scatter in the flight data is present and is represented by high and low values for each flight condition. The separation between high and low data points gives some indication of the pilot workload required for that flight condition.

For all the wind speeds it is seen that higher tail rotor collective (lower % pedal position from full left pedal) is required for right sideward flight (RSF, around 90° heading) and lower collective is needed in left sideward flight (LSF, around 270° heading). This is due to the change in the inflow velocity at the tail rotor as heading angle varies. The occurrence of the vortex ring state in left sideward flight is seen as an increase in the tail rotor collective required. The analysis shows the onset of vortex ring state at about 25 knots (Figure 22) as a dip in the curve around 270°. At higher wind velocities, this phenomenon becomes more pronounced. The data show a large range between high and low pedal position near 270° for wind speeds above 25 knots which is characteristic of the thrust oscillations present in the vortex ring state.

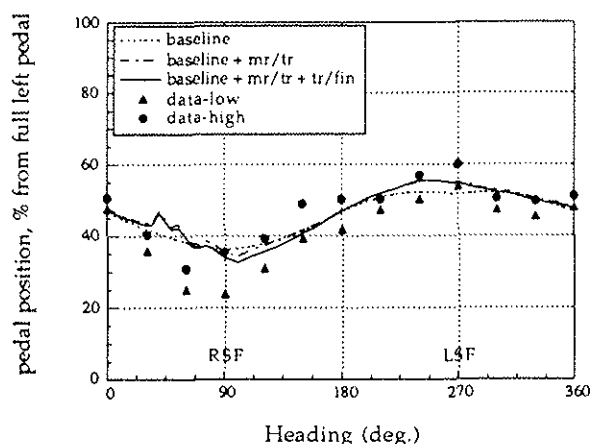


Fig. 21 SH-2 critical azimuth results compared with flight test data (speed = 20 knots)

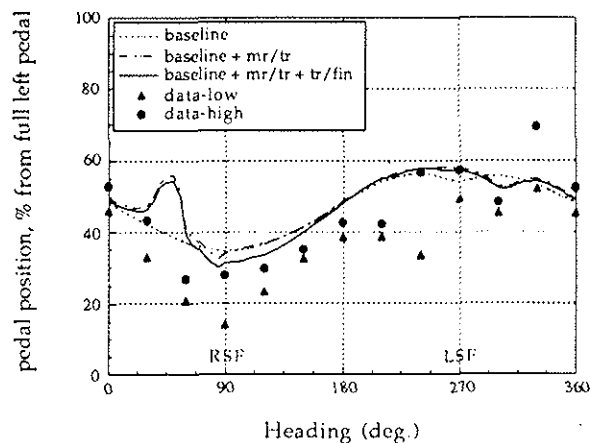


Fig. 22 SH-2 critical azimuth results compared with flight test data (speed = 25 knots)

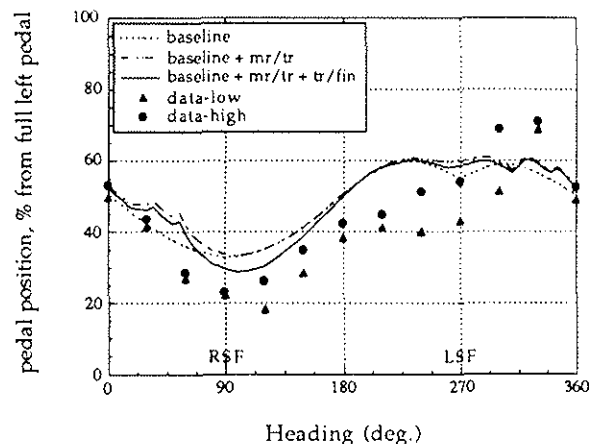


Fig. 23 SH-2 critical azimuth results compared with flight test data (speed = 30 knots)

The calculated effect of the main rotor wake on the tail rotor is very pronounced around heading angles of 40° to 50° (Figure 22) and around 300° to 330° (Figures 24 and 25). This phenomenon is due to the main rotor tip vortices rolling-up and impinging on the tail rotor at these heading angles. The effect of the advancing side tip vortex (U.S. rotors) impinging on the tail rotor (around 40° to 50° heading) is most predominant at 25 knots and decreases in intensity as wind speed increases to 45 knots. The retreating side vortex effect, as predicted by analysis, becomes noticeable at 35 knots and is more prominent at 45 knots. The effect of both the advancing and retreating side main rotor tip vortices is to increase tail rotor thrust which is evident in the figures as a reduction in left pedal input (higher % from full left). This beneficial effect has also been observed in wind tunnel tests [5, 7]. The data show the retreating side vortex effect for wind speeds of 25 knots and greater. No data were available at 45° heading angle where the predicted advancing side vortex effect is most pronounced. Figures 21 to 25 show that the main rotor tip vortex interaction effect is very sensitive to heading angle. A slight change in wind heading can cause a sudden change in aircraft yaw moment.

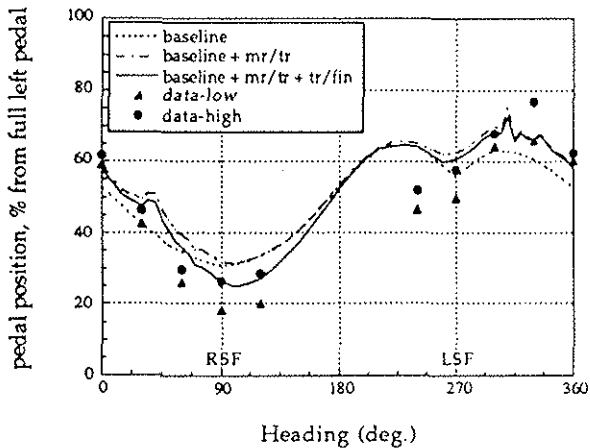


Fig. 24 SH-2 critical azimuth results compared with flight test data (speed = 35 knots)

The tail rotor/fin interactions (the difference in the figures between the solid and dash-dotted lines) are, as expected, more pronounced in right sideward flight than in left sideward flight. These interactions are also much greater as wind speed increases. The figures show that tail rotor/fin interactions may need to be modeled in greater detail since some differences between

the predictions and test data exist particularly in right sideward flight.

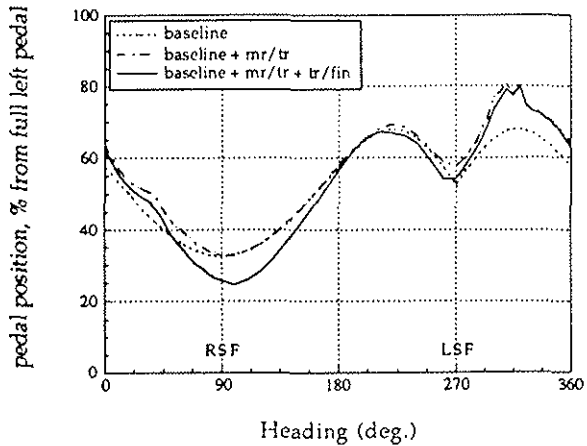


Fig. 25 SH-2 critical azimuth results (speed = 45 knots) - no flight test data available

The location and effect of the main rotor tip vortices is very sensitive to several factors such as airspeed, sidewind, rate of climb/descent and aircraft pitch attitude. To better understand the flow environment near the tail rotor location velocity vector plots were generated on a vertical surface 1.2045R behind the main rotor hub which corresponds to the location of the tail rotor hub with respect to the main rotor. These plots help visualize the predicted flow field around the tail rotor. The tail rotor hub is located 0.13R below the main rotor hub line.

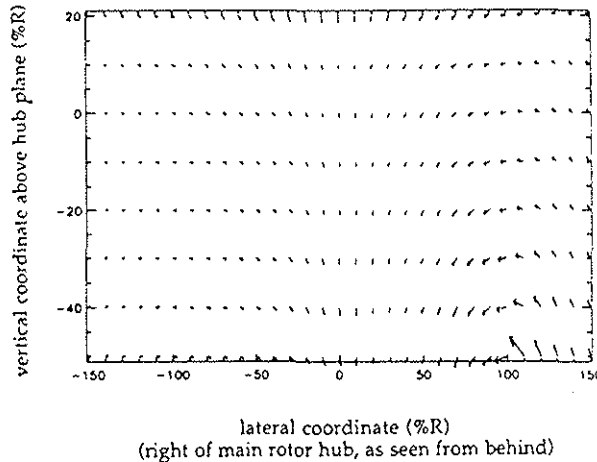


Fig. 26 Velocity vector plot 1.2045R behind the SH-2 main rotor hub (speed = 20 knots,  $\mu = 0.05$ )

At a speed of 20 knots (Figure 26), the main rotor wake is just beginning to influence the flow around the tail rotor location. The main rotor tip vortices are well below the main rotor

and are not close to rolling up at this advance ratio of 0.05. Hence the wake effects at the tail rotor at this speed are negligible (Figure 21) due to the localized influence of the individual blade tip vortices.

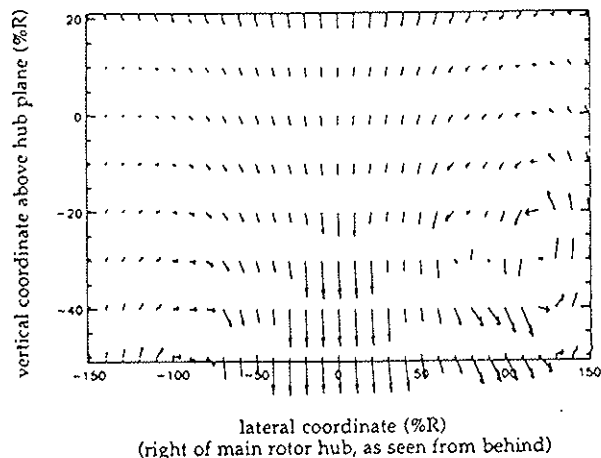


Fig. 27 Velocity vector plot 1.2045R behind the SH-2 main rotor hub (speed = 35 knots,  $\mu = 0.086$ )

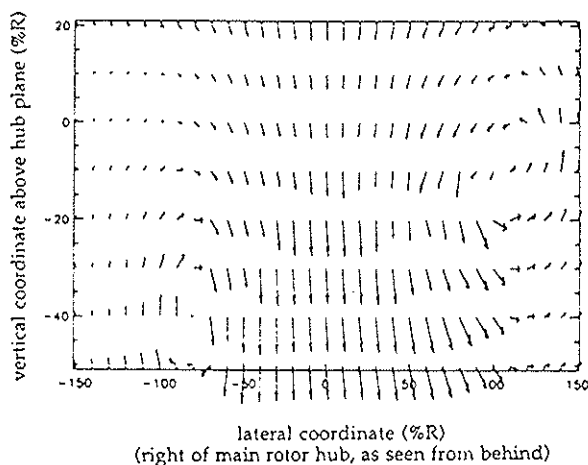


Fig. 28 Velocity vector plot 1.2045R behind the SH-2 main rotor hub (speed = 45 knots,  $\mu = 0.11$ )

Figure 27 shows the flow picture at a speed of 35 knots (corresponding to an advance ratio of 0.086). At this speed, there is a considerable effect of the main rotor wake at the tail rotor location. At 45 knots (Figure 28,  $\mu=0.11$ ), the two tip vortices are well formed. The advancing side vortex is at the hub plane, whereas the retreating side vortex is below the hub plane, close to the location of the tail rotor hub. Hence a larger effect of the main rotor wake is seen in the pedal position predictions around heading angle of  $315^\circ$  than is seen around the  $45^\circ$  heading at 45 knots (Figure 25). The variation in the pedal positions with heading at this higher speed (Figure 25) is also

more gradual compared to the trends seen at lower speeds.

## CONCLUSIONS

Based on the results obtained in this work, the following conclusions are made:

1. The SH-2 servo-flap controlled helicopter is modeled in UMARC and the predicted trim controls correlate well with existing flight data.
2. Main rotor wake induced velocities predicted using the free wake model in UMARC correlate satisfactorily with model test data below and behind the main rotor. The trends in the induced velocities are predicted satisfactorily but the magnitudes are generally under predicted.
3. The predictions of isolated tail rotor thrust coefficient using the comprehensive tail rotor model are very good for hover and most wind velocities and wind azimuths. The overall trend of the vortex ring state and the effect of edgewise flow is captured reasonably well using a momentum based tail rotor inflow model.
4. The empirical tail rotor/vertical fin interaction model captures the basic blockage and adverse fin force effects. These interactions affect the tail rotor thrust considerably above 25 knots in right sideward flight.
5. Prediction of critical azimuth results (pedal position with varying heading) for different airspeeds correlate satisfactorily with available flight test data.
6. A significant effect of the main rotor wake at the tail rotor is observed for heading angles of  $40^\circ$  to  $50^\circ$  and  $300^\circ$  to  $330^\circ$ . These effects are due to the main rotor rolled-up tip vortices impinging on the tail rotor.
7. The predicted effect of the main rotor tip vortices is beneficial in that it increases tail rotor thrust; however, this effect is very sensitive to heading angle. A slight change in heading angle can result in a sudden change in aircraft yaw moment due to rapid changes in tail rotor thrust.
8. More work is still needed in the area of main rotor/tail rotor interactions and in the modeling of the tail rotor/vertical fin interactions.

## ACKNOWLEDGMENTS

This research work was supported by the Naval Air Systems Command, LCDR David Lee, and the technical monitor was Mr. Jonah Ottensoser. The authors also acknowledge Mr. Herman Kolwey, NAWC, Patuxent River, for providing flight test data and for technical discussion regarding the SH-2 flight tests.

## REFERENCES

1. Brocklehurst, Alan., "A Significant Improvement to the Low Speed Yaw Control of the Sea King using a Tail Boom Strake," *Proceedings of the Eleventh European Rotorcraft Forum*, Paper No.32, London, England, Sep. 1985.
2. Kloppel, V., Huber, H., and Enenkl, B., "Development of Bearingless Tail Rotors," *Proceedings of the Sixteenth European Rotorcraft Forum*, Glasgow, Scotland, Sep. 1990.
3. Ellin, Lt.A.D.S., RN, "Tail Rotor Aerodynamic Features Recorded in Flight," *Proceedings of the Sixteenth European Rotorcraft Forum*, Glasgow, Scotland, Sep. 1990.
4. Mouille, R., "The 'Fenestron' Shrouded Tail Rotor of the SA.341 Gazelle," *Journal of the American Helicopter Society*, Oct. 1970.
5. Wiesner, W. and Kohler, G., "Tail Rotor Performance in Presence of Main Rotor, Ground, and Winds," *Proceeding of the 29th Annual Forum of the American Helicopter Society*, May 1973.
6. Snellen, D.M., "OH-58 Loss of Tail Rotor Effectiveness," *U.S. Army Aviation Digest*, pp. 31-35, Sept. 1984.
7. Blake, B.B., Hodder, D.J., and Hanker, E.J., "Wind Tunnel Investigation into the Directional Control Characteristics of an OH-58 Helicopter," USAAVRADCOM TR-83-D-18, June 1984.
8. Cress, J.P., "Tail Rotor Trickery," *Approach*, June 1980.
9. Wallace, L.A., "Tail Rotor Trickery: A Case of Loss of Authority," *Approach*, May 1991.
10. Kolwey, H.G., "Analysis Tools Derived From Investigating Aerodynamic Loss of Tail Rotor Effectiveness," *Paper presented at the Society of Flight Test Engineers 22nd Annual Symposium*, Aug., 1991.
11. Ellin, A.D., and Brown, D.C., "RAE Bedford Tail Rotor Aerodynamic Flight Research Program Lynx AH MK 5 Trial Conduct," *Paper presented at the Society of Flight Test Engineers Workshop on Rotorcraft Flight Testing*, Patuxent River, MD, Sept., 1991.
12. Wilson, J.C., and Kelley, H.L., "Measured Aerodynamic Forces on Three Typical Helicopter Tail Boom Cross Sections," *Journal of the American Helicopter Society*, Vol. 28, (4), Oct. 1983.
13. Kelley, H.L., Crowell, C.A., Yenni, K.R., and Lance, M.B., "Flight Investigation of the Effect of Tail Boom Strakes on Helicopter Directional Control," *Journal of the American Helicopter Society*, Vol. 37, (2), April 1992.
14. Bir, G., Chopra, I., and Nguyen, K., "Development of UMARC (University of Maryland Advanced Rotor Code)," *Proceedings of the 46th Annual Forum of the American Helicopter Society*, Washington, D.C., May 1990, pp.55-70.
15. Wei, F.S., and Jones, R., "Correlation and Analysis for SH-2F 101 Rotor," *Journal of Aircraft*, Vol. 35, No. 7, July 1988.
16. "Technical Description Data for the Kaman 101 Rotor Blade on the SH-2F Helicopter," Report No. R-1815, Kaman Aerospace Corporation, Bloomfield, CT, Oct. 1985.
17. Abbott, I.H., and Doenhoff, A.E.v., *Theory of Wing Sections*, Dover Publications, Inc., New York, 1959, pp. 188-220.
18. Johnson, W., "A Comprehensive Analytical Model of Rotorcraft Aerodynamics & Dynamics, Part I: Analysis Development," NASA TM-81182, July 1980.
19. Scully, M.P., "Computation of Helicopter Rotor Wake Geometry and its Influence on Rotor Harmonic Airloads," ASRL TR 178-1, Massachusetts Institute of Technology, March 1975.
20. Torok, M.S., and Chopra, I., "Hingeless Rotor Aeroelastic Stability Analysis with Refined Aerodynamic Modeling," *Journal of the American Helicopter Society*, Oct. 1991, pp. 48-56.

21. Johnson, W., "Airloads, Wakes, and Aeroelasticity," NASA CR-177551, April 1990.
22. Bi, N., "Contributions to the Experimental Investigation of Rotor/Body Aerodynamic Interactions," Ph.D. Thesis, University of Maryland, May 1991.
23. Johnson, W., *Helicopter Theory*, Princeton University Press, 1980.
24. Sheridan, P.F., Hanker, E.J.Jr., and Blake, B.B., "A Study of the Aerodynamic Interactions of the Tail Rotor and Fin," Boeing Vertol Company, May 1983.
25. Hanker, E.J.Jr., and Smith, R.P., "Parameters Affecting Helicopter Interactional Aerodynamics in Ground Effect," *Proceedings of the 39th Annual Forum of the American Helicopter Society*, St. Louis, May 1983,
26. Prouty, R.W., *Helicopter Performance, Stability and Control*, Robert E. Krieger Publishing Company, Inc., 1990, pp. 283-287.